

## IV-TUNING: PARAMETER-EFFICIENT TRANSFER LEARNING FOR INFRARED-VISIBLE TASKS

Yaming Zhang<sup>1</sup>, Chenqiang Gao<sup>2\*</sup>, Fangcen Liu<sup>1</sup>, Junjie Guo<sup>1</sup>, Lan Wang<sup>3</sup>, Xinggan Peng<sup>4</sup>, Deyu Meng<sup>5</sup>

<sup>1</sup> Chongqing University of Posts and Telecommunications, <sup>2</sup> Sun Yat-sen University,

<sup>3</sup> Michigan State University, <sup>4</sup> Nanyang Technological University, <sup>5</sup> Xi'an Jiaotong University

### ABSTRACT

Existing infrared and visible (IR-VIS) methods inherit the general representations of Pre-trained Visual Models (PVMs) to facilitate complementary learning. However, our analysis indicates that the commonly-used full fine-tuning paradigm leads to a constrained, low-rank feature space, which has proved to seriously impair generalization. One solution is freezing parameters to preserve pre-trained knowledge and thus maintain diversity of the feature space. To this end, we propose IV-tuning, a parameter-efficient method to adapt PVMs to various IR-VIS downstream tasks, including salient object detection, semantic segmentation, and object detection. Compared with the full fine-tuning baselines and existing IR-VIS methods, IV-tuning facilitates the learning of complementary information between infrared and visible modalities with less than 3% of the backbone parameters, and effectively alleviates the overfitting problem. The code is available in <https://github.com/Yummy198913/IV-tuning>.

**Index Terms**— Parameter-Efficient Transfer Learning, infrared and visible tasks, Overfitting.

### 1. INTRODUCTION

In recent years, transformer-based pre-trained visual models (PVMs), such as ViT [1], Swin Transformer [2], et al., have been widely introduced into infrared-visible (IR-VIS) tasks [3, 4]. Albeit effective, the resulting models are costly to train, hard to scale, and prone to overfitting—especially given the small datasets typical of the IR-VIS community [5, 6].

From a modern viewpoint, the scaling law [7] suggests that on a smaller dataset, performance stops improving as model parameters increase, leading to overfitting. To investigate this, we analyze the behavior of feature space via Principal Component Analysis (PCA) under full fine-tuning (FFT) and freezing paradigms. As shown in Fig. 2: as the network depth increases, the FFT model initially captures diverse signals but quickly collapses into a highly constrained and low-rank<sup>1</sup> subspace, where **a single principal component captures almost all effective information**<sup>2</sup>. This aligns with early information-bottleneck studies of neural networks [8, 9] that *overfitting is largely due to the compression phase and low-rank feature spaces hinder generalization by memorizing trivial patterns*.

One potential remedy to address the overfitting problem is freezing the parameters. As shown in Fig. 2 (b), the frozen PVM rapidly expands the input feature space after the first layer, leading to a more

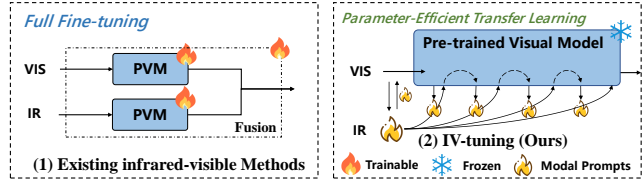


**Fig. 1:** Existing infrared-visible (IR-VIS) methods typically extend Pre-trained Visual Models (PVMs) into a dual branch network and perform full fine-tuning, while we propose a streamlined paradigm where the utilization of infrared can be greatly simplified.

expressive representation, but fails to capture task-specific discriminative information. Therefore, Parameter-Efficient Transfer Learning (PETL) introduces lightweight modules on top of frozen models, such as inserting adapters [10, 11] or learnable prompts [12, 13], offering a favorable adaptation pathway.

Visually, the infrared images exhibit distinct thermal radiation between objects and background. Such thermal structures correspond to low-frequency variations in the frequency domain. To quantify this, we analyze the energy distributions<sup>3</sup> of both modalities, revealing that infrared features possess stronger low-frequency energy while sharing mid-to-high-frequency characteristics with visible images (Fig. 3 (a)). This indicates that infrared low-frequency components need preservation, yet common convolution operations (e.g.,  $3 \times 3$  convolution), due to their limited receptive fields, weaken the low-frequency signal, as shown in Fig. 3 (b). In contrast, linear projection preserves low-frequency information through global transformation, making it particularly suitable for integrating infrared priors into frozen PVMs in a parameter-efficient manner.

To this end, we propose IV-tuning, a parameter-efficient method for adapting PVMs to various IR-VIS tasks. As illustrated in Fig. 1 (2), instead of adding an extra backbone, IV-tuning introduces cascade modal prompts to the frozen PVMs, which inherit the general representations of PVMs to the maximum extent. At its core, IV-tuning leverages cascaded Modality-aware Prompter (MP) blocks to generate and inject visual prompts into the frozen PVM. Furthermore, we observe a sharp decline in feature rank after the first PVM layer (Fig. 2 (b) 0.293 vs. 0.126). To mitigate this discrepancy, we propose two fusion strategies, referred to as  $\alpha$ -fusion and  $\beta$ -fusion.

Extensive experiments demonstrate that by training less than 3% of the backbone parameters, IV-tuning significantly outperforms full fine-tuning baselines and previous methods across multiple IR-VIS tasks, including salient object detection, semantic segmentation, and object detection.

<sup>1</sup>The “rank” here means the number of significant principal components.

<sup>2</sup>In PCA, it refers to variance captured by principal components. Larger eigenvalues indicate components explaining more variance and contributing more to data representation.

<sup>3</sup>The “energy” here is defined as the sum of Fourier magnitudes within each radial frequency band, normalized to form a distribution. It reflects the proportion of information across different frequency components.

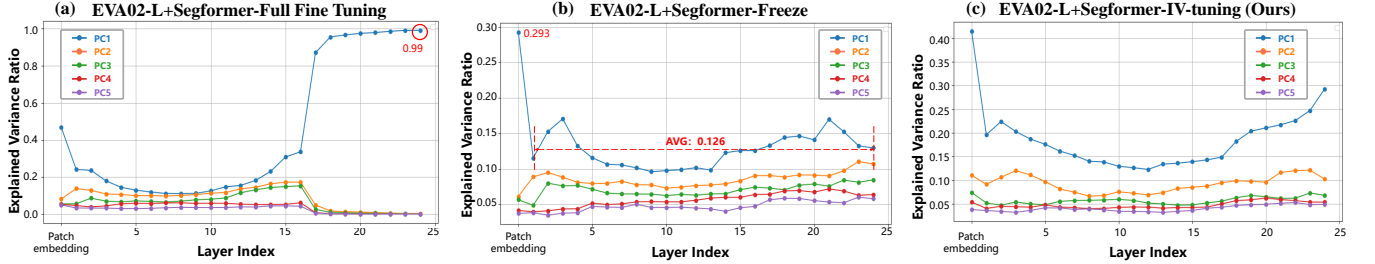


**Fig. 2: Observation of effective information contained in the feature space via Principal Component Analysis (PCA).** We visualize the explained variance ratio of top five principal components across layers with EVA02-L+Segformer. Results show that: (a) the full fine-tuning collapses features into a low-rank subspace, thereby sacrificing generalization. (b) the frozen models retain diversity but struggle to extract task-specific discriminative information. In contrast, our method preserves diversity while effectively capturing discriminative information.

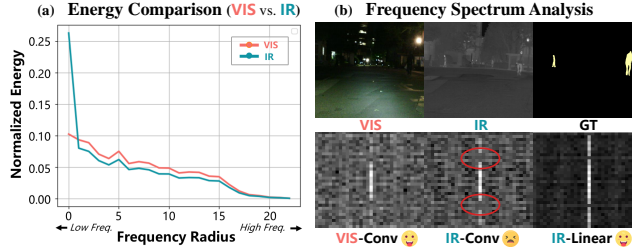


**Fig. 3: Analysis of energy distribution between infrared and visible modalities, and frequency spectral patterns under varying conditions,** where the center and corners denote low and high frequencies, respectively, we calculate the average distribution of energy on the MFNet [6] dataset. We show that (a) infrared images exhibit stronger low-frequency energy, while sharing mid-to-high-frequency similarities with visible images. (b) convolution enhances high-frequency details (e.g., edges) in visible images, but attenuates low-frequency signals in infrared images, which are critical for complementary learning. In contrast, simple linear projection can effectively capture low-frequency signals in the infrared modality, which inspires the motivation behind our design.

## 2. RELATED WORK

Previous IR-VIS methods [14, 3, 4] have demonstrated the effectiveness of harnessing Pre-trained Visual Models (PVMs). These approaches routinely employ dual-branch backbones and full fine-tune these models on IR-VIS datasets. However, in addition to scalability issues caused by the dual-branch design, few works have investigated the intrinsic differences between infrared and visible modalities or addressed the overfitting risks introduced by PVMs.

Recent advances in Parameter-Efficient Transfer Learning (PETL), such as prompt-tuning [12, 13] and adapter-tuning [10, 11], mitigate these issues by optimizing only a minimal set of parameters on frozen backbones. Nonetheless, most PETL methods focus on the visible modality or single-task scenarios. A generalized and efficient PETL approach that incorporates modality-aware mechanisms is therefore critical to advancing IR-VIS learning.

## 3. METHODOLOGY

### 3.1. Overall Architecture

Compared to visible tasks, the infrared-visible tasks introduce an additional infrared input  $\mathbf{x}_{ir}$ , which is aligned and synchronized with the visible input  $\mathbf{x}_{vis}$ . The goal is to learn a mapping  $F$ :

$\{\mathbf{x}_{vis}, \mathbf{x}_{ir}\} \rightarrow \mathbf{p}$ , where  $F = \phi \circ f$ . Here,  $f$  is a transformer-based Pre-trained Visual Model (PVM) which includes norm layer  $LN(\cdot)$ , Multi-head Self-Attention  $Attn(\cdot)$  and Feed-Forward Network  $FFN(\cdot)$ , and  $\phi$  is a task-specific prediction head.

To inject infrared knowledge, we extract prompt tokens  $\mathbf{z}_{\mathcal{P}}$  from  $\mathbf{x}_{ir}$  via a patch embedding layer. These are fed into a Modality-aware Prompter- $\alpha$  (MP- $\alpha$ , denoted as  $\mathcal{P}_{\alpha}$ ) to produce the initial prompt  $\mathcal{P}^0$ .

Within each encoder layer  $\mathcal{E}^l$  ( $l = 1, 2, 3, \dots, L$ ), we insert two weight-sharing MP- $\beta$  blocks ( $\mathcal{P}_{\beta}$ ) after the  $Attn$  layer and  $FFN$  layer, respectively, to progressively refine the backbone feature. Denoting the input to layer  $\mathcal{E}^l$  as  $\mathbf{z}^{l-1}$ , the process of the  $l$ -th encoder layer can be formulated as:

$$\mathbf{z}^l = FFN(Attn(\mathbf{z}^{l-1}) + \mathcal{P}^{l_1}) + \mathcal{P}^{l_2}, \quad (1)$$

where the  $\mathcal{P}^{l_1}$  and  $\mathcal{P}^{l_2}$  are the output of the blocks MP- $\beta^{l_1}$  and MP- $\beta^{l_2}$ , respectively. The output of each encoder layer updates the initial modal prompt for next layer. The final token sequence  $\mathbf{z}^L$ , obtained after  $L$  encoder layers, is subsequently passed to the decoder  $\phi$  to generate the prediction:  $\mathbf{p} = \phi(\mathbf{z}^L)$ .

### 3.2. Modality-aware Prompter

In light of our PCA analysis shown in Fig. 2, we propose the Modality-aware Prompter (MP), which consists of MP- $\alpha$  and MP- $\beta$  blocks. Both blocks project features into a low-rank subspace to extract principal components and apply modality-specific operations, though they employ different fusion strategies. The forward process begins with a Simple Feature Transform (SFT) that normalizes and recalibrates the visible and prompt tokens channel-wise:

$$\mathbf{z}'_{vis} = LN_1(\mathbf{z}) \odot \omega_1 + \phi_1, \quad (2)$$

$$\mathbf{z}'_{\mathcal{P}} = LN_2(\mathbf{z}) \odot \omega_2 + \phi_2, \quad (3)$$

where  $\omega$  and  $\phi$  are learnable parameters, and  $\odot$  denotes the element-wise multiplication. The transformed features  $\mathbf{z}'_{vis}$  and  $\mathbf{z}'_{\mathcal{P}}$  are then projected into a latent space via linear layers  $s_1(\cdot)$  and  $s_2(\cdot)$  to generate latent representations  $\mathcal{M}_{vis}$  and  $\mathcal{M}_{\mathcal{P}}$ :

$$\mathcal{M}_{vis} = s_1(\mathbf{z}'_{vis}); \quad \mathcal{M}_{\mathcal{P}} = s_2(\mathbf{z}'_{\mathcal{P}}). \quad (4)$$

**Modality-aware process:** We apply modality-specific processing after down projections. For visible features  $\mathcal{M}_{vis}$ , a Hybrid Operation (HO) enhances discriminative signals: the features are split, processed via a  $3 \times 3$  depth-wise convolution and concatenated, then aggregated using  $1 \times 1$  convolutions to yield  $\mathcal{M}_{vis}^e$ . The infrared features  $\mathcal{M}_{\mathcal{P}}$  remain unchanged to preserve semantic integrity.

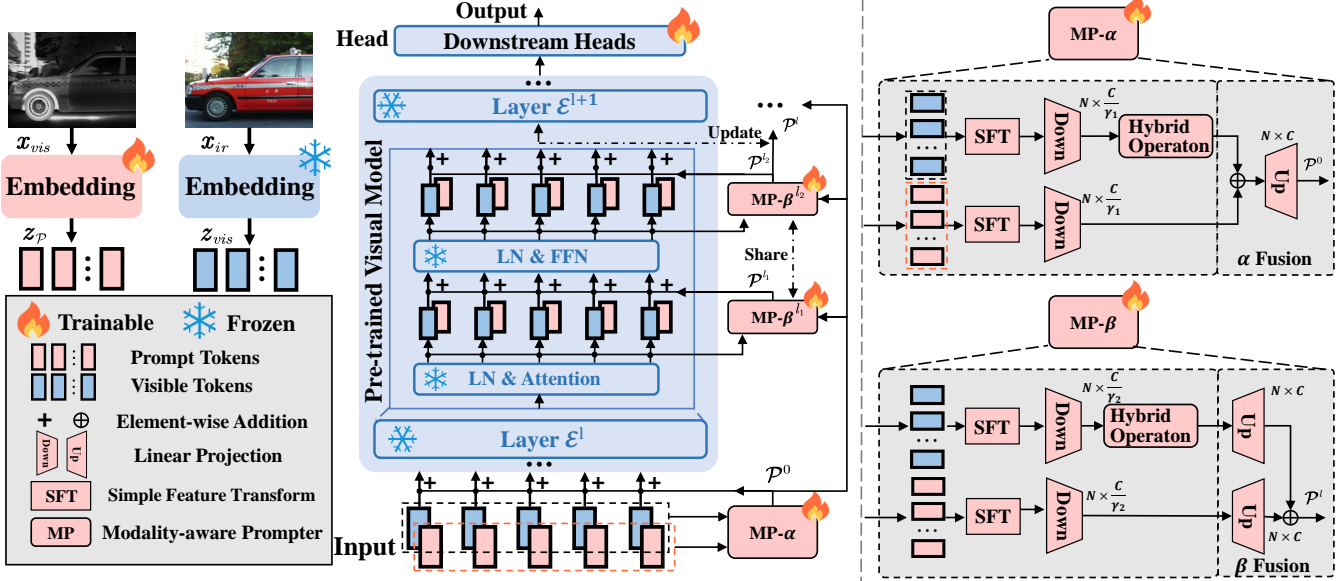


Fig. 4: The overview of the proposed IV-tuning.

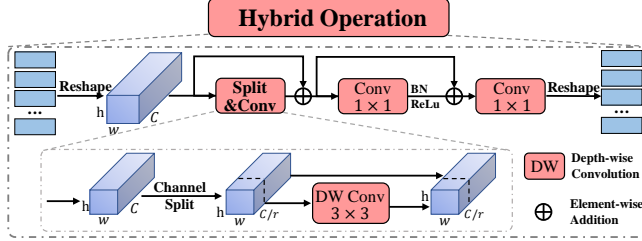


Fig. 5: Detailed design of the Hybrid Operation. The input tokens are reshaped to feature maps, then a depth-wise  $3 \times 3$  convolution applied to selected channels with residual connection, followed by two  $1 \times 1$  convolution layers with batch normalization and ReLu activation in between. We set the split ratio  $\frac{1}{r}$  as  $\frac{1}{4}$  by default.

**Rank-aware Fusion Strategies:** The PCA results indicate that the feature space within the PVMs becomes more diversified, suggesting that varying degrees of fusion flexibility should be allocated to features at different stages. Accordingly, we employ distinct latent dimensions and fusion strategies to accommodate this variability: in MP- $\alpha$ , features are fused directly in the low-dimensional latent space, while in MP- $\beta$ , each modality is first projected back to the original dimension  $C$  before fusion to preserve feature specificity:

$$\mathcal{P}^0 = s_3(\mathcal{M}_{vis}^e + \mathcal{M}_P); \mathcal{P}^l = s_3(\mathcal{M}_{vis}^e) + s_4(\mathcal{M}_P), \quad (5)$$

where  $s_3(\cdot)$  and  $s_4(\cdot)$  are the same as  $s_1(\cdot)$  and  $s_2(\cdot)$ . The generated prompts are integrated into the backbone via element-wise addition. All MP- $\beta$  blocks share parameters within the same encoder layer, effectively reducing parameters without compromising performance.

### 3.3. Optimization

During tuning, we freeze the entire PVM and optimize only a small set of parameters  $\theta = \{\tau^{ir}, \mathcal{P}_\alpha, \{\mathcal{P}_\beta^l\}_{l=1}^L, \phi\}$ , where  $\tau^{ir}$  is the infrared patch embedding layer. The objective is formulated as:

$$\theta_{IV-tuning} = \arg \min_{\theta} \frac{1}{|\mathcal{D}|} \sum \mathcal{L}(\phi(z^L, y)), \quad (6)$$

where  $\mathcal{D}$  is the IR-VIS dataset and  $\mathcal{L}$  is the task-specific loss function, which is consistent with the full fine-tuning setup.

## 4. EXPERIMENTS

**Datasets:** (1) For salient object detection, we evaluate our method on the VT821 [15], VT1000 [16] and VT5000 [17] datasets. We use the S-measure ( $S_\alpha$ ), weighted F-measure ( $F_\beta^\omega$ ), E-measure ( $E_m$ ) and mean absolute error ( $MAE$ ). (2) For semantic segmentation, we report the results on the widely used MFNet [6] dataset. The mean Intersection over Union ( $mIoU$ ) is used for evaluation. (3) For object detection, we provide the comparison results on the M3FD [5] dataset. The  $mAP$ ,  $mAP50$ , and  $mAP75$  are employed for evaluation.

**Pre-trained Visual Models and Decoders:** For salient object detection and semantic segmentation, we use CPNet [28] and Segformer [29] as decoders, respectively, with vanilla Swin Transformer [2] and EVA02 [30] as the PVMs. For object detection, we only use the widely adopted Swin Transformer [2] as the PVM, and select CO-DETR [31] and DINO [32] as the detectors. To balance precision and efficiency, we employ the large version of these architectures.

**Implementation Details:** (1) For salient object detection, we use Adam ( $lr = 5e-5$ , weight decay =  $1e-1$ ) and train for 200 epochs with a batch size of 8 on  $384 \times 384$  cropped images. (2) For semantic segmentation, we use SGD ( $lr = 1e-3$ , weight decay =  $1e-2$ ) and train for 160,000 iterations with a batch size of 2 on  $512 \times 512$  cropped images. (3) For object detection, we use AdamW ( $lr = 1e-4$ , weight decay =  $1e-4$ ) and train for 48 epochs with a batch size of 2 on  $640 \times 640$  cropped images. The baseline method is constructed by fully fine-tuning the model using only the visible modality. All experiments are conducted on the RTX 3090 with identical settings for fairness.

**Experimental Results:** By breaking the constraints of dual-branch architectures, IV-tuning efficiently leverages larger and more powerful pre-trained models for superior performance. As shown in Tab. 1, the EVA02 baseline performs competitively against UniRGB-IR [21] on VT1000, confirming the strong transferability of PVMs. With extra infrared input, IV-tuning further improves performance using fewer trainable parameters, and beats all previous IR-VIS methods and full fine-tuning baselines. For semantic segmentation, IV-tuning surpasses all state-of-the-art methods, improving  $mIoU$  by 10.3% (EVA02-L) and 6.4% (Swin-L) with minimal trainable parameters. For object detection, IV-tuning achieves the highest  $mAP$  of 62.1% using only 5.0M trainable parameters.

**Table 1:** Overall performance on the IR-VIS salient object detection. The trainable parameters in backbones (#TP), S-mesure ( $S_\alpha$ ), weighted F-mesure ( $F_\beta^\omega$ ), E-mesure ( $E_m$ ) and mean absolute error ( $MAE$ ) are reported. We use  $\times 2$  denotes a dual-branch backbone model.

Methods	Publications	#TP (M)	VT821 [15]				VT1000 [16]				VT5000 [17]			
			$S_\alpha \uparrow$	$F_\beta^\omega \uparrow$	$E_m \uparrow$	$MAE \downarrow$	$S_\alpha \uparrow$	$F_\beta^\omega \uparrow$	$E_m \uparrow$	$MAE \downarrow$	$S_\alpha \uparrow$	$F_\beta^\omega \uparrow$	$E_m \uparrow$	$MAE \downarrow$
CAVER [18]	TIP 23	44.5 $\times 2$	0.898	0.845	-	0.027	0.938	0.911	-	0.017	0.899	0.849	-	0.028
SACNet [19]	TMM 24	192.5 $\times 2$	0.908	0.861	-	0.024	0.946	0.929	-	0.014	0.919	0.888	-	0.020
TCE [20]	TCE 24	192.5 $\times 2$	0.915	0.874	0.939	0.023	0.943	0.919	0.966	0.016	0.917	0.875	0.943	0.024
UniRGB-IR [21]	ACMM 25	8.9	0.881	-	0.039	0.939	-	-	0.018	0.906	-	-	0.027	-
ConTriNet [22]	TPAMI 25	192.5 $\times 2$	0.917	0.878	0.941	0.022	0.942	0.925	0.956	0.014	0.926	0.898	0.957	0.020
Swin-L+CPNet (baseline)	IJCV 24	192.5	0.890	0.831	0.917	0.033	0.939	0.918	0.966	0.015	0.911	0.873	0.949	0.025
<b>+IV-tuning (Ours)</b>	-	<b>5.0</b>	<b>0.904</b>	<b>0.848</b>	<b>0.928</b>	<b>0.029</b>	<b>0.940</b>	<b>0.915</b>	<b>0.964</b>	<b>0.016</b>	<b>0.917</b>	<b>0.884</b>	<b>0.957</b>	<b>0.022</b>
EVA02-L+CPNet (baseline)	IJCV 24	304.2	0.890	0.832	0.915	0.034	0.938	0.915	0.959	0.017	0.907	0.866	0.943	0.026
<b>+IV-tuning (Ours)</b>	-	<b>7.6</b>	<b>0.924</b>	<b>0.890</b>	<b>0.951</b>	<b>0.021</b>	<b>0.948</b>	<b>0.931</b>	<b>0.971</b>	<b>0.012</b>	<b>0.931</b>	<b>0.904</b>	<b>0.964</b>	<b>0.019</b>

**Table 2:** Overall performance on the MFNet [6] and M3FD [5] dataset for IR-VIS semantic segmentation and object detection.

(a) Overall performance on the IR-VIS semantic segmentation.

Methods	Publications	#TP (M)	mIoU	
			mIoU (%)	#TP (M)
RSFNet [23]	ICCV 23	11.7 $\times 2$	54.60	
CDDFuse [4]	CVPR 23	42.5 $\times 2$	44.50	
CMX [24]	T-ITS 23	64.0 $\times 2$	59.70	
CAINet [25]	TMM 24	3.4 $\times 2$	58.60	
UniRGB-IR [21]	ACMM 25	8.9	59.30	
EVA02-L+Segformer (baseline)	NeurIPS 21	304.2	54.53	
<b>+IV-tuning (Ours)</b>	-	<b>7.6</b>	<b>60.14</b>	
Swin-L+Segformer (baseline)	NeurIPS 21	192.5	56.78	
<b>+IV-tuning (Ours)</b>	-	<b>5.0</b>	<b>60.44</b>	

(b) Overall performance on the IR-VIS object detection.

Methods	Publications	#TP (M)	mAP			
			mAP	mAP@50	mAP@75	
TarDAL [5]	CVPR 22	86.3 $\times 2$	54.5	80.9	-	
CDDFuse [4]	CVPR 23	86.3 $\times 2$	54.6	81.1	57.0	
CBAM [26]	WACV 24	77.0 $\times 2$	50.5	81.0	-	
CoCoNet [27]	IJCV 24	86.3 $\times 2$	54.2	80.7	-	
ICAFusion [3]	PR 24	86.3 $\times 2$	59.9	89.2	65.0	
Swin-L+DINO (baseline)	ICRL 23	192.5	60.1	90.8	64.0	
<b>+IV-tuning (Ours)</b>	-	<b>5.0</b>	<b>61.2</b>	<b>90.9</b>	<b>66.6</b>	
Swin-L+CÖ-DETR (baseline)	ICCV 23	192.5	60.5	91.0	64.1	
<b>+IV-tuning (Ours)</b>	-	<b>5.0</b>	<b>62.1</b>	<b>91.7</b>	<b>65.9</b>	

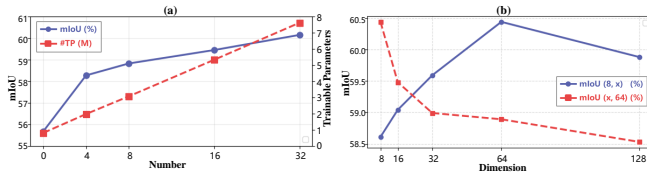


**Fig. 6:** Influence on the number of MP- $\beta$  blocks and dimensions.

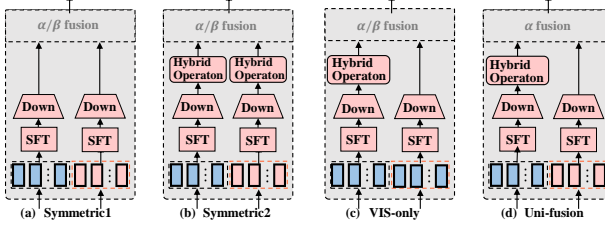


**Fig. 7:** Variants of MP blocks.

**Comparison with visible-based PETL methods:** We compare IV-tuning with existing visible-domain PETL methods on the MFNet [6] dataset with Swin-L+Segformer [2, 29]. As shown in Tab. 3, most PETL methods outperform the two baselines, which indicates that PETL methods are promising and efficient fine-tuning solutions to IR-VIS tasks. Tailored for IR-VIS tasks, the proposed IV-tuning achieves even superior performance, surpassing previous PETL methods and full fine-tuning.

**Ablation Study:** As shown in Fig. 7, variant analyses on MFNet validate our design: (a and b) Adding convolution to the infrared flow impairs performance, indicating that convolutions may damage effective information in the infrared modality. (c) When the infrared is missing, our method degrades to a visible PETL method, yet still outperforms the FFT baseline. (d) A unified fusion strategy degrades performance (59.07 vs. 60.44), demonstrating the necessity of tailored fusion for different feature spaces. As shown in Fig. 6 (a), further experiments show that inserting more MP- $\beta$  blocks consistently improves results. Larger dimensions benefit MP- $\beta$ , but harm MP- $\alpha$ , indicating that compact dimensions suffice in low-rank spaces, whereas diverse spaces require greater representation flexibility.

**Table 3:** Comparisons with visible-based PETL methods.

Methods	Publications	#TP (M)	FFT	Freeze	+VPT	+AdaptFormer	+LoRA	+Rein	+IV-tuning (Ours)
			(baseline)	(baseline)	[13]	[10]	[11]	[33]	
#TP (M)		192.5	0.0	0.2	2.3	1.2	14.7	5.0	
mIoU		56.78	53.02	49.79	56.79	58.14	57.83	<b>60.44</b>	

**Table 4:** Variants of Modality-aware Prompter.

(a) Symmetric1	(b) Symmetric2	(c) VIS-only	(d) Uni-fusion	IV-tuning	
				#TP (M)	mIoU
4.82	5.23	5.23	3.46	5.03	<b>60.44</b>
59.31	58.98	56.82	59.07		

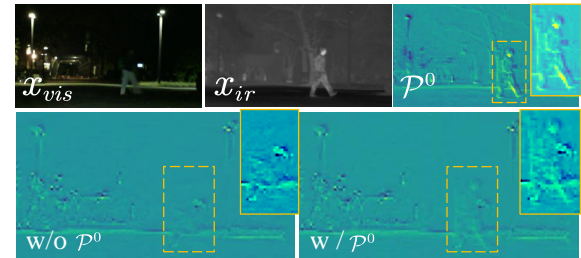


**Fig. 8:** Visualization of the prompting process.

**Visualization:** Fig. 8 illustrates our prompting process. Under the challenging nighttime scenario where the pedestrian is blurred, the modal prompt  $\mathcal{P}^0$  effectively integrates infrared information to refine the backbone features, thereby improving performance.

## 5. CONCLUSION

This paper investigates the generalization bottlenecks in infrared-visible tasks, and proposes the IV-tuning framework that centers on the Modality-aware Prompter, which applies modality-specific prompting and tailored fusion strategies to address cross-modal discrepancies. Without complex architectural modifications, IV-tuning adapts PVMs to the multimodal domain with minimal parameters. Extensive experiments across multiple benchmarks demonstrate the effectiveness, efficiency, and strong generalization ability of our method.

## 6. REFERENCES

[1] Alexey Dosovitskiy, “An image is worth 16x16 words: Transformers for image recognition at scale,” *arXiv preprint arXiv:2010.11929*, 2020.

[2] Ze Liu, Yutong Lin, Yue Cao, Han Hu, Yixuan Wei, Zheng Zhang, Stephen Lin, and Baining Guo, “Swin transformer: Hierarchical vision transformer using shifted windows,” in *Proceedings of the IEEE/CVF international conference on computer vision*, 2021, pp. 10012–10022.

[3] Jifeng Shen, Yifei Chen, Yue Liu, Xin Zuo, Heng Fan, and Wankou Yang, “Icafusion: Iterative cross-attention guided feature fusion for multispectral object detection,” *Pattern Recognition*, vol. 145, pp. 109913, 2024.

[4] Zixiang Zhao, Haowen Bai, Jianguo Zhang, Yulun Zhang, Shuang Xu, Zudi Lin, Radu Timofte, and Luc Van Gool, “Cddfuse: Correlation-driven dual-branch feature decomposition for multi-modality image fusion,” in *Proceedings of the IEEE/CVF conference on computer vision and pattern recognition*, 2023, pp. 5906–5916.

[5] Jinyuan Liu, Xin Fan, Zhanbo Huang, Guanyao Wu, Risheng Liu, Wei Zhong, and Zhongxuan Luo, “Target-aware dual adversarial learning and a multi-scenario multi-modality benchmark to fuse infrared and visible for object detection,” in *Proceedings of the IEEE/CVF Conference on Computer Vision and Pattern Recognition*, 2022, pp. 5802–5811.

[6] Qishen Ha, Kohei Watanabe, Takumi Karasawa, Yoshitaka Ushiku, and Tatsuya Harada, “Mfnet: Towards real-time semantic segmentation for autonomous vehicles with multi-spectral scenes,” in *2017 IEEE/RSJ International Conference on Intelligent Robots and Systems (IROS)*. IEEE, 2017, pp. 5108–5115.

[7] Jared Kaplan, Sam McCandlish, Tom Henighan, Tom B Brown, Benjamin Chess, Rewon Child, Scott Gray, Alec Radford, Jeffrey Wu, and Dario Amodei, “Scaling laws for neural language models,” *arXiv preprint arXiv:2001.08361*, 2020.

[8] Ravid Shwartz-Ziv and Naftali Tishby, “Opening the black box of deep neural networks via information,” 2017.

[9] Suriya Gunasekar, Blake E Woodworth, Srinadh Bhojanapalli, Behnam Neyshabur, and Nati Srebro, “Implicit regularization in matrix factorization,” *Advances in neural information processing systems*, vol. 30, 2017.

[10] Shoufa Chen, Chongjian Ge, Zhan Tong, Jiangliu Wang, Yibing Song, Jue Wang, and Ping Luo, “Adaptformer: Adapting vision transformers for scalable visual recognition,” *Advances in Neural Information Processing Systems*, vol. 35, pp. 16664–16678, 2022.

[11] Edward J Hu, Yelong Shen, Phillip Wallis, Zeyuan Allen-Zhu, Yuanzhi Li, Shean Wang, Lu Wang, and Weizhu Chen, “Lora: Low-rank adaptation of large language models,” *arXiv preprint arXiv:2106.09685*, 2021.

[12] Jiawen Zhu, Simiao Lai, Xin Chen, Dong Wang, and Huchuan Lu, “Visual prompt multi-modal tracking,” in *Proceedings of the IEEE/CVF conference on computer vision and pattern recognition*, 2023, pp. 9516–9526.

[13] Menglin Jia, Luming Tang, Bor-Chun Chen, Claire Cardie, Serge Belongie, Bharath Hariharan, and Ser-Nam Lim, “Visual prompt tuning,” in *European Conference on Computer Vision*. Springer, 2022, pp. 709–727.

[14] Lihua Jian, Songlei Xiong, Han Yan, Xiaoguang Niu, Shaowu Wu, and Di Zhang, “Rethinking cross-attention for infrared and visible image fusion,” *arXiv preprint arXiv:2401.11675*, 2024.

[15] Jin Tang, Dongzhe Fan, Xiaoxiao Wang, Zhengzheng Tu, and Chenglong Li, “Rgbd salient object detection: Benchmark and a novel cooperative ranking approach,” *IEEE Transactions on Circuits and Systems for Video Technology*, vol. 30, no. 12, pp. 4421–4433, 2019.

[16] Zhengzheng Tu, Tian Xia, Chenglong Li, Xiaoxiao Wang, Yan Ma, and Jin Tang, “Rgbd image saliency detection via collaborative graph learning,” *IEEE Transactions on Multimedia*, vol. 22, no. 1, pp. 160–173, 2019.

[17] Zhengzheng Tu, Yan Ma, Zhun Li, Chenglong Li, Jieming Xu, and Yongtao Liu, “Rgbd salient object detection: A large-scale dataset and benchmark,” *IEEE Transactions on Multimedia*, vol. 25, pp. 4163–4176, 2022.

[18] Youwei Pang, Xiaoqi Zhao, Lihe Zhang, and Huchuan Lu, “Caver: Cross-modal view-mixed transformer for bi-modal salient object detection,” *IEEE Transactions on Image Processing*, vol. 32, pp. 892–904, 2023.

[19] Kunpeng Wang, Danying Lin, Chenglong Li, Zhengzheng Tu, and Bin Luo, “Alignment-free rgbd salient object detection: Semantics-guided asymmetric correlation network and a unified benchmark,” *IEEE Transactions on Multimedia*, 2024.

[20] Chengtao Lv, Xiaofei Zhou, Bin Wan, Shuai Wang, Yaoqi Sun, Jiyong Zhang, and Chenggang Yan, “Transformer-based cross-modal integration network for rgbd salient object detection,” *IEEE Transactions on Consumer Electronics*, 2024.

[21] Maoxun Yuan, Bo Cui, Tianyi Zhao, and Xingxing Wei, “Unirgb-ir: A unified framework for visible-infrared downstream tasks via adapter tuning,” *arXiv preprint arXiv:2404.17360*, 2024.

[22] Hao Tang, Zechao Li, Dong Zhang, Shengfeng He, and Jinhui Tang, “Divide-and-conquer: Confluent triple-flow network for rgbd salient object detection,” *IEEE Transactions on Pattern Analysis and Machine Intelligence*, 2024.

[23] Ping Li, Junjie Chen, Binbin Lin, and Xianghua Xu, “Residual spatial fusion network for rgbd-thermal semantic segmentation,” *Neurocomputing*, vol. 595, pp. 127913, 2024.

[24] Jiaming Zhang, Huayao Liu, Kailun Yang, Xinxin Hu, Ruiping Liu, and Rainer Stiefelhagen, “Cmx: Cross-modal fusion for rgbd semantic segmentation with transformers,” *IEEE Transactions on intelligent transportation systems*, 2023.

[25] Ying Lv, Zhi Liu, Bin Li, Gongyang, and Zhang, “Context-aware interaction network for rgbd semantic segmentation,” *IEEE Transactions on Multimedia*, vol. 26, pp. 6348–6360, 2024.

[26] Sri Aditya Deevi, Connor Lee, Lu Gan, Sushruth Nagesh, Gaurav Pandey, and Soon-Jo Chung, “Rgbd object detection via scene-specific fusion modules,” in *Proceedings of the IEEE/CVF Winter Conference on Applications of Computer Vision*, 2024, pp. 7366–7375.

[27] Jinyuan Liu, Runjia Lin, Guanyao Wu, Risheng Liu, Zhongxuan Luo, and Xin Fan, “Coconet: Coupled contrastive learning network with multi-level feature ensemble for multi-modality image fusion,” *International Journal of Computer Vision*, pp. 1–28, 2023.

[28] Xihang Hu, Fuming Sun, Jing Sun, Fasheng Wang, and Haojie Li, “Cross-modal fusion and progressive decoding network for rgbd salient object detection,” *International Journal of Computer Vision*, pp. 1–19, 2024.

[29] Enze Xie, Wenhui Wang, Zhiding Yu, Anima Anandkumar, Jose M Alvarez, and Ping Luo, “Segformer: Simple and efficient design for semantic segmentation with transformers,” *Advances in neural information processing systems*, vol. 34, pp. 12077–12090, 2021.

[30] Yuxin Fang, Quan Sun, Xinggang Wang, Tiejun Huang, Xinlong Wang, and Yue Cao, “Eva-02: A visual representation for neon genesis,” *Image and Vision Computing*, vol. 149, pp. 105171, 2024.

[31] Zhuofan Zong, Guanglu Song, Lei Liu, Yu, Hang Su, and Zhu, “Dets with collaborative hybrid assignments training,” in *Proceedings of the IEEE/CVF international conference on computer vision*, 2023, pp. 6748–6758.

[32] Hao Zhang, Feng Li, Shilong Liu, Lei Zhang, Hang Su, Jun Zhu, Lionel M Ni, and Heung-Yeung Shum, “Dino: Detr with improved denoising anchor boxes for end-to-end object detection,” *arXiv preprint arXiv:2203.03605*, 2022.

[33] Zhixiang Wei, Lin Chen, Yi Jin, Xiaoxiao Ma, Tianle Liu, Pengyang Ling, Ben Wang, Huaian Chen, and Jinjin Zheng, “Stronger fewer & superior: Harnessing vision foundation models for domain generalized semantic segmentation,” in *Proceedings of the IEEE/CVF Conference on Computer Vision and Pattern Recognition*, 2024, pp. 28619–28630.